Received: 5 June 2020 | Accepted: 26 November 2020

DOI: 10.1002/pamm.202000035

Phase Field Simulations of Wetting Based on Molecular Simulations

Felix Diewald[1,*], **Michaela Heier**[2], **Martin Lautenschläger**[2], **Charlotte Kuhn**[3], **Kai Langenbach**[2], **Hans Hasse**[2], and **Ralf Müller**[1]

[1] Institute of Applied Mechanics, TU Kaiserslautern, 67653 Kaiserslautern, Germany
[2] Laboratory of Engineering Thermodynamics, TU Kaiserslautern, 67653 Kaiserslautern, Germany
[3] Faculty 7, University of Stuttgart, 70569 Stuttgart, Germany

Manufacturing techniques that can produce surfaces with a defined microstructure are in the focus of current research efforts. The ability to manufacture such surfaces gives rise to the need for numerical models that can predict the wetting properties of a given microstructure and can help to optimize these surfaces with respect to certain wetting properties. The present phase field (PF) model for wetting is linked to molecular dynamics (MD) simulations by the usage of the MD based perturbed Lennard-Jones truncated and shifted (PeTS) equation of state as well as a MD based viscosity correlation. The lower computational effort of the PF simulations compared to MD simulations enables the model to simulate wetting scenarios on the microscale.

1 Phase Field Model

The present phase field (PF) model represents a coupling of the static PF model described in [1] with the compressible Navier-Stokes equations, cf. [2]. It can be classified as a Navier-Stokes-Korteweg model. Considering a domain $\mathcal{B}$ (bounded by $\partial\mathcal{B}$) the mass and momentum balances,

$$\dot{\rho} + \rho \mathrm{div}\vec{v} = 0 \qquad \text{in} \qquad \mathcal{B} \qquad \text{and} \qquad \rho\dot{\vec{v}} = \mathrm{div}\boldsymbol{\sigma} \qquad \text{in} \qquad \mathcal{B}\,, \tag{1}$$

are solved for particle density $\rho(\vec{x},t)$ and velocity $\vec{v}(\vec{x},t)$. The coupling is ensured via the constitutive relation for the stress tensor $\boldsymbol{\sigma}$, for details see [2]. Position in space and time are denoted by $\vec{x}$ and t. The material time derivative is denoted by $\dot{(\cdot)} = \frac{\mathrm{d}(\cdot)}{\mathrm{d}t}$. Gravitational effects are neglected. The boundary conditions read

$$\vec{v} = \vec{0} \qquad \text{on} \qquad \partial\mathcal{B} \qquad , \tag{2}$$

$$\kappa\nabla\rho\cdot\vec{n} + \frac{\gamma_{\mathrm{sf}}}{\rho'-\rho''}\left(30\varphi^4 - 60\varphi^3 + 30\varphi^2\right) = 0 \qquad \text{on} \qquad \partial\mathcal{B}\cap\partial\mathcal{B}_s \qquad \text{, and} \tag{3}$$

$$\nabla\rho\cdot\vec{n} = 0 \qquad \text{on} \qquad \partial\mathcal{B}\backslash\partial\mathcal{B}_s \qquad , \tag{4}$$

with the outer normal to the boundary $\vec{n}$ and $\partial\mathcal{B}_s$ as the part of $\partial\mathcal{B}$ that is given by a solid surface. The parameter κ is taken from the PeTS equation of state [3,4]. The boundary condition (3) with $\varphi = \frac{\rho-\rho''}{\rho'-\rho''}$, where ρ' and ρ'' are the liquid and vapor bulk densities, ensures a specified contact angle Θ for a droplet that is in contact with $\partial\mathcal{B}_s$, cf. [5,6]. The solid-fluid surface tension is given by $\gamma_{\mathrm{sf}} = \gamma_{\mathrm{sl}} - \gamma_{\mathrm{sv}}$, where γ_{sl} and γ_{sv} are the solid-liquid and solid-vapor surface tensions. The temperature T is assumed to be constant. The backward Euler method is used for the time discretization. For more details on the model and its numerical implementation, the reader is referred to [2].

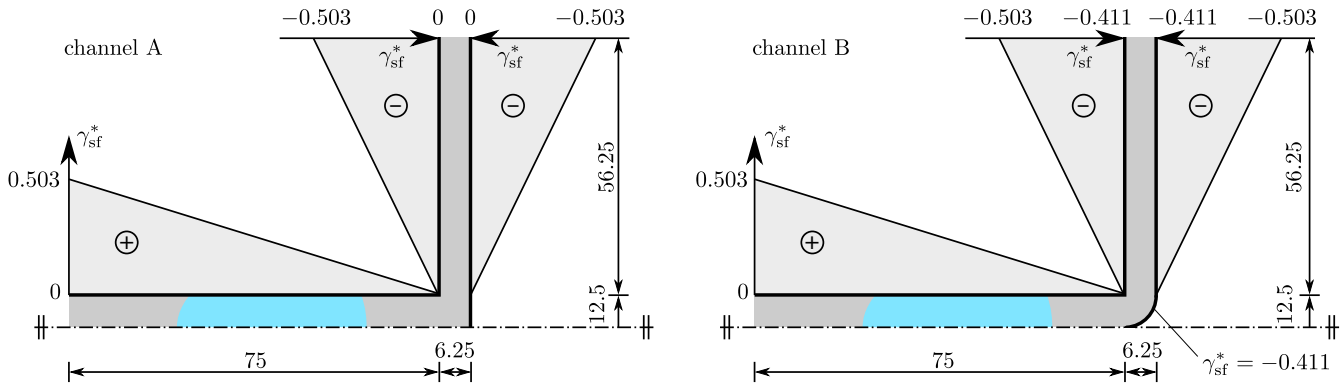

Fig. 1: Sketch of channel A (left) and channel B (right). Both channels show a gradient of the solid-fluid surface tension γ_{sf}.

* Corresponding author: e-mail fdiewald@rhrk.uni-kl.de, phone +49 (0) 631 205 3781, fax +49 (0) 631 205 2128

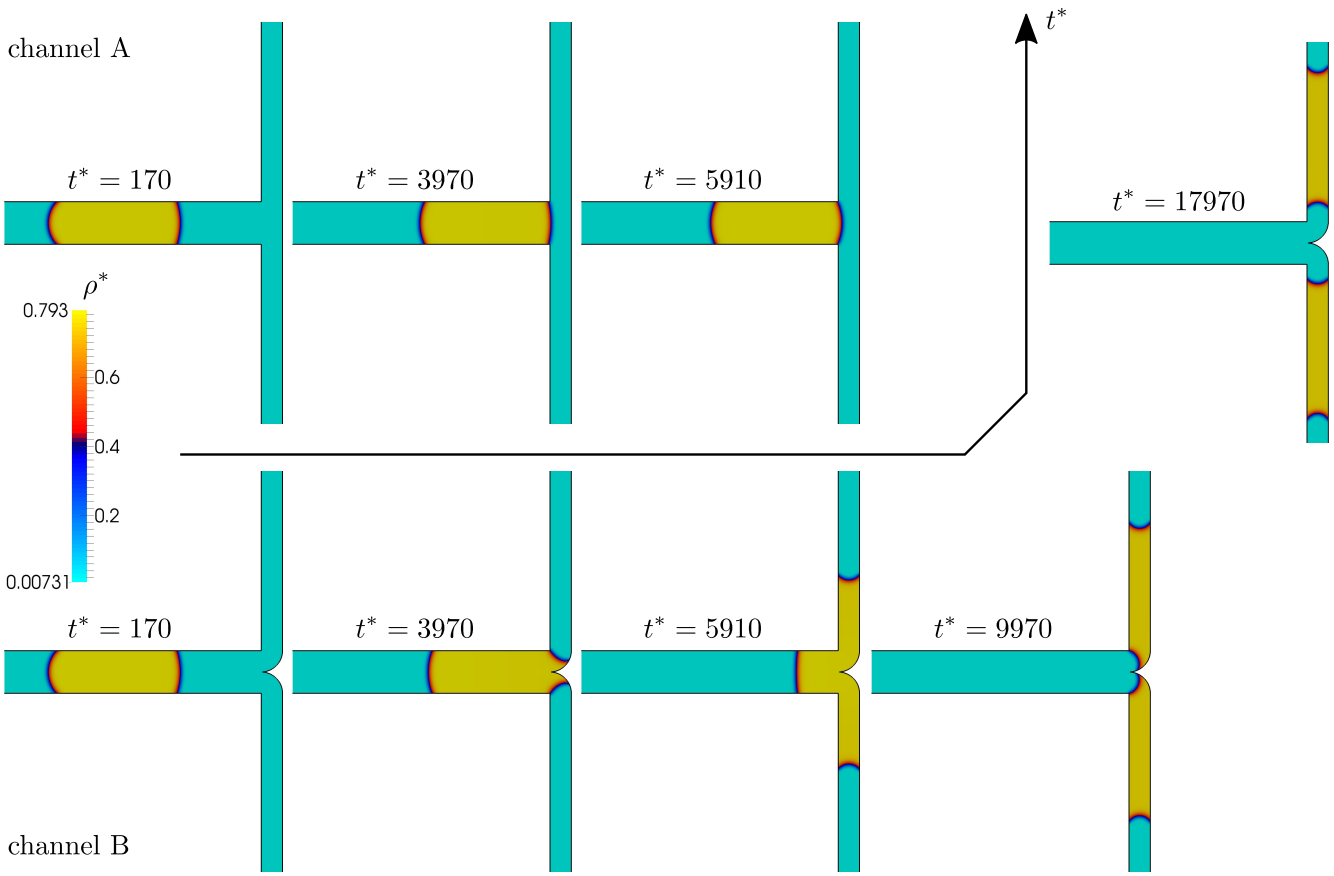

Fig. 2: Temporal evolution of a droplet in channel A and channel B. The droplet in channel A does not pass the junction. The droplet in channel B passes the junction.

2 Numerical Examples

The temporal evolution of a droplet in two different channels with a gradient of the solid-fluid surface tension γ_{sf} is investigated. Fig. 1 shows a sketch of the two channels (channel A and channel B) presenting the slope of γ_{sf} and the channels' dimensions. While the sketch only shows a symmetric representation of the channels, the computational domains contains the full geometry. All physical quantities are nondimensionalized by the size and energy parameter of the Lennard-Jones potential σ^{LJ} and $\varepsilon^{\mathrm{LJ}}$ as well as by the mass per particle M^{LJ}, cf. [2]. The nondimensionalized quantities are marked by an asterisk. A droplet of equal size is placed inside both channels. The initial velocity in the entire computational domain is $\vec{v}^*_{\mathrm{ini}} = \vec{0}$ and the temperature is $T^* = 0.7$. At this temperature the liquid-vapor surface tension is $\gamma^*_{\mathrm{lv}} = 0.581$ [1]. Therefore, the values of γ_{sf} shown in Fig. 1 lead to theoretical contact angles between $\Theta_{\mathrm{max}} = 150°$ and $\Theta_{\mathrm{min}} = 30°$, cf. Young's equation $\Theta = \arccos(\frac{\gamma_{\mathrm{sv}} - \gamma_{\mathrm{sl}}}{\gamma_{\mathrm{lv}}})$. Fig. 2 shows the temporal evolution of the droplet in channel A and channel B. At $t^* = 170$ the results for the two channels are identical. The temporal evolution starts to differ once the droplet reaches the end of the horizontal part of the channel. In channel A, the droplet does not pass the junction and its motion is stopped. In channel B, the droplet passes the junction, splits into two droplets of equal size, and both droplets continue their motion through the channel. A more detailed investigation of the presented and also other channel types can support the design of lab-on-a-chip devices.

Acknowledgements This research was funded by the Deutsche Forschungsgemeinschaft (DFG, German Research Foundation) – Projektnummer 172116086 – SFB 926.
Open access funding enabled and organized by Projekt DEAL.

References

[1] F. Diewald, M. Heier, M. Horsch, C. Kuhn, K. Langenbach, H. Hasse, R. Müller, J. Chem. Phys. **149**, 064701 (2018).
[2] F. Diewald, M. P. Lautenschlaeger, S. Stephan, K. Langenbach, C. Kuhn, S. Seckler, H.-J. Bungartz, H. Hasse, R. Müller, Comput. Meth. Appl. Mech. Eng. **361**, 112773 (2020).
[3] M. Heier, S. Stephan, J. Lui, W. G. Chapman, H. Hasse, K. Langenbach, Mol. Phys. **116**, 2083-2094 (2018).
[4] S. Stephan, J. Liu, K. Langenbach, W. G. Chapman, H. Hasse, J. Phys. Chem. C **122**, 24705-24715 (2018).
[5] M. Ben Said, M. Selzer, B. Nestler, D. Braun, C. Greiner, H. Garcke, Langmuir **30**, 4033-4039 (2014).
[6] F. Diewald, C. Kuhn, M. Heier, K. Langenbach, M. Horsch, H. Hasse, R. Müller, Comp. Mater. Sci. **141**, 185-192 (2018).